Analysis of micromachined Fabry-Pérot cavities using phase-sensitive optical low coherence interferometry: Insight on dimensional measurements of dielectric layers

M. Malak,[1,a] A.-F. Obaton,[2] F. Marty,[1] N. Pavy,[1] S. Didelon,[1] P. Basset,[1] and T. Bourouina[1]

[1]*Université Paris-Est, Laboratoire ESYCOM, ESIEE Paris, Cité Descartes, 2 Boulevard Blaise Pascal, 93162 Noisy-le-Grand Cedex, France*

[2]*(LNE), Laboratoire Commun de Métrologie, 29 avenue R. Hennequin, 78197 Trappes Cedex, France*

(Received 27 February 2012; accepted 17 May 2012; published online 4 June 2012)

Herein, we highlight a behavior underlying the physics of Fabry-Pérot micro-cavities with distributed reflectors as there is a need to discriminate between effective and physical cavity lengths. Hence, Phase-Sensitive Optical Low Coherence Interferometry has been implemented to characterize micro-cavities with planar or curved reflectors. Beside the retrieved physical length, we obtain valuable information about the reflector thickness and number of layers. The accuracy of the technique has been estimated. Results suggest that this technique might be suitable to retrieve dimensional characteristics of any device constructed from multiple dielectric layers, whose thickness ranges from 2 micrometers up to hundreds of micrometers. [http://dx.doi.org/10.1063/1.4727741]

After the introduction of Bragg gratings more than a century ago[1] and besides their primary use for the study of diffraction-related phenomena, they were also involved in a huge number of microscopic optical components, including fiber Bragg gratings,[2] corrugated waveguides[3] and Distributed Feedback lasers.[4,5] Similarly, Bragg mirrors have a periodic structure, most often obtained from multiple-stack, thin-film coatings. Their interesting performances made them popular in various applications where they were used either as anti-reflection coatings or, on the contrary, as high reflectance mirrors. These applications include Vertical Cavity Surface Emitting Lasers (VCSELs),[6,7] thin-film optical filters[8] and micromachined Fabry-Pérot (FP) cavities.[9–12] Hence, the mirror evolved from being a thin metallic coating localized at the vicinity of the coated surface, to a non-localized reflector, distributed over a finite thickness range. Then, our attention was focused on studying the impact of this specific geometrical detail to acquire a better understanding of devices involving distributed reflectors.

A closer look to the micromachined FP cavities[9–12] reveals that the cavity length is not only small but it eventually became comparable to the thicknesses of the Bragg reflectors layers, which cannot be neglected anymore as they play an important role in the device physics. This situation is also encountered in semiconductor lasers including VCSELs where the cavity length L is between a few micrometers and even several hundreds of micrometers while the mirror thickness t falls in the (sub-)micrometer range. The impact of these geometrical parameters is manifested experimentally, with an actual *effective cavity length*, L_{eff}, quite different from the *physical length* of the cavity L_{phys}. Though this concept of effective length was thoroughly studied in several micro-photonic components involving combinations of semiconductor and air layers,[13,14] the situation is quite different in our case because the change of materials is concentrated at the vicinity of the mirror,

[a]Corresponding author: malakkam@esiee.fr

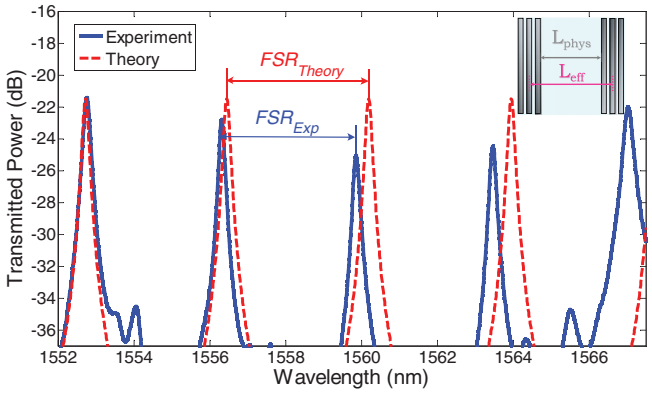

FIG. 1. Comparison between the expected spectral response and the experimental spectral response which have different FSRs in the wavelength domain. The inset shows a schematic illustration of FP cavity with planar distributed Bragg reflectors. The arrows point out to the effective length L_{eff} and the physical length L_{phys}.

which consists here of silicon-air Bragg reflectors. In other words, one can define in our case, two virtual interfaces inside the Bragg reflector stacks and the resonating optical cavity behaves as if light bounces between these virtual interfaces. An important consequence is that the experimental value of the Free Spectral Range $FSR_{Exp}(f)$, which describes the periodicity of the cavity response in the frequency domain, can no longer be used to retrieve the cavity physical length L_{phys}. Instead, one only obtains the effective length L_{eff} from the relation $L_{eff} = c/2nFSR_{Exp}(f)$, c being the speed of light in free space and n is the refractive index of the cavity media. This phenomenon is illustrated in Fig. 1, where a difference between the obtained $FSR_{Exp}(\lambda)$ $(= \lambda^2/2nL_{eff})$ and the expected $FSR_{Theory}(\lambda)$ $(= \lambda^2/2nL_{phys})$ is observed (here in the wavelength domain). Referring to Fig. 1, we find that L_{phys} of the cavity is 324 μm while L_{eff} of the cavity is 342 μm, exhibiting a 5.5% increase with respect to the expected theoretical value.

A schematic illustration is presented in the inset of Fig. 1. to support the idea where the introduced parameter L_{eff} is drawn inside the Bragg reflector and it is larger than L_{phys}. It is to be noted that the device presented in Fig. 2. is somewhat different from the ideal case and it pertains to a FP cavity with curved reflectors; it represents practically a more interesting configuration than FP cavities with planar reflectors, especially with its cavity length exceeding 10 μm. Indeed, the improved stability of the curved cavity enables one to combine simultaneously a long cavity length ($>$ 200 μm) and large Q-factor ($\sim$ 9000), as demonstrated in a recent report.[12] However, in this special case, one needs to refer to $<L_{eff}>$ and $<L_{phys}>$ as the average effective length and the average physical length, respectively, over the light spot area having a finite size. This length variation is mainly related to the reflector radius of curvature R and the spot size D.

Motivated by the need to discriminate between the effective length L_{eff} and the physical length L_{phys} in Fabry-Perot cavities based on distributed Bragg reflectors and whose cavity lengths exceed 200 μm, we proceeded to an analysis, which takes advantage of the technique of Phase Sensitive Optical Low Coherence Interferometry (PS-OLCI).[15,16] The corresponding setup used in our experiments is shown in Fig. 3. The basic principle of an Optical Low Coherence Interferometer is based on a Michelson interferometer coupled to a broadband (low coherence) source operating in the near-infrared range. This enables achieving high spatial resolution in the measurements. As in a conventional Michelson interferometer, there is a movable mirror in the reference arm enabling the variation of the optical path difference between the reference and test arms of the system, δ. To retrieve the actual position of this movable mirror, the setup includes a highly coherent visible light Michelson reflectometer, whose reference arm is commonly shared by the low coherent interferometer. This strategy guarantees the synchronisation of the two signals at any acquisition speed as well as the retrieval of information in the spatial domain, that is the interferograms, corresponding to the responses of the Device Under Test (DUT) as a function of the displacement δ and hence, the optical path difference. These interferograms correspond to the real part of the inverse Fourier transform of

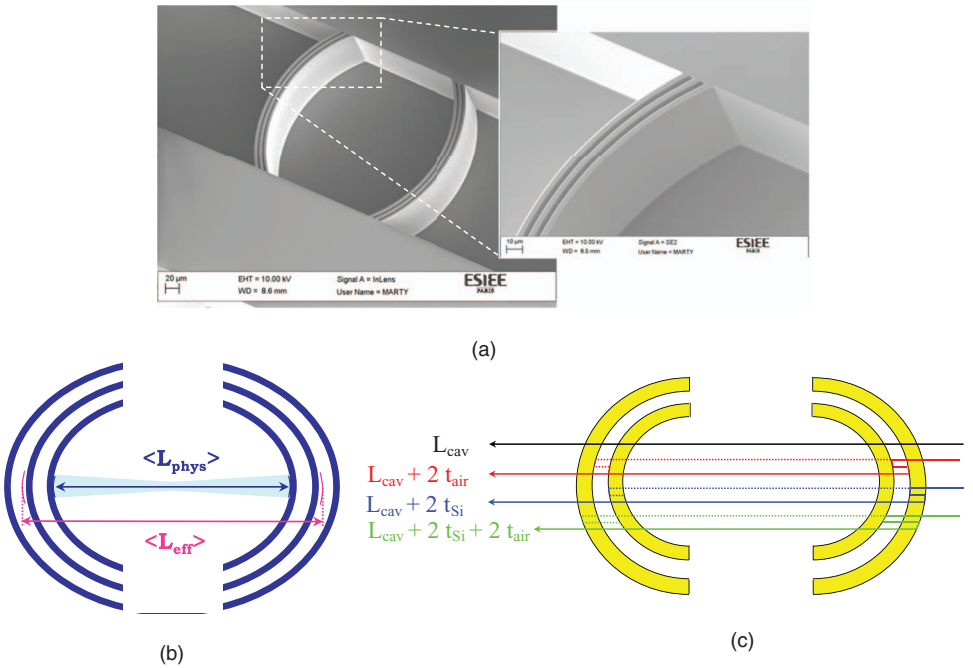

FIG. 2. (a) SEM photos of a sample based on three Bragg layers per mirror (whose cavity length $L_{phys} = 210\ \mu$m) overall view showing the full cavity and its L_{phys}, the inset is a close view showing the details of a Bragg reflector. (b) Schematic representation of curved FP cavity illustrating the averaged lengths $<L_{eff}>$ and $<L_{phys}>$. (c) Schematic illustration of the various reflection schemes taking place inside a curved FP cavity based on two silicon layers per mirror which explains the source of the different peaks that arise in the spatial interferograms as graphed in Fig. 4. Only some paths are traced for the shake of simplicity.

the product of the source spectrum $S(\sigma)$ by the amplitude response $\tilde{F}(\sigma)$ of the device under test, namely,

$$I(\delta) = \mathrm{Re}\left\{\int_{-\infty}^{+\infty} S(\sigma)\tilde{F}(\sigma)\exp(j2\pi\sigma\delta)d\sigma\right\} \quad (1)$$

where σ is the wavenumber (corresponding to the inverse of the wavelength). As the response acquisition is synchronized with the displacement of the movable mirror controlled with sub-wavelength accuracy, Fourier transform can be performed on the interferograms. Thus the system enables to recover also information in the spectral domain: amplitude and phase spectrum as a function of the wavelength, corresponding to light propagating into the DUT. Therefore, this scheme allows recovering both spatial and spectral domains responses of an optical device. Its versatility enables the study of guided wave components[17] as well as those based on free space propagation of light, as discussed in this paper. It is worth to mention that the proposed technique deployed for the analysis of Fabry-Perot cavities is limited to the characterization of optical lengths exceeding half the coherence length of the broadband source (15 μm here). For silicon, this limitation corresponds to layer thickness larger than 2 μm. Cavity physical lengths exceeding 500 μm can also be retrieved as demonstrated in the experimental study presented hereafter. From this point of view, the proposed methodology is very complementary to the ellipsometric technique, adopted for much thinner layers.

Firstly, a curved FP cavity based on three silicon Bragg layers per mirror (Device 1) has been studied using the PS-OLCI technique. The detailed dimensional characteristics of this FP cavity are given in the first row of table I. These dimensions, used as reference, were measured using a Scanning Electron Microscope (SEM) at normal incidence angle. SEM photos of Device 1 are shown in Fig. 2. The DUT has been inserted in one of the arms of the OLCI as shown in Fig. 3. The light is coupled into and from the device using lensed fibers mounted onto precision alignment positioners. It is to be noted that in the case of the curved cavities under consideration, we have to take into

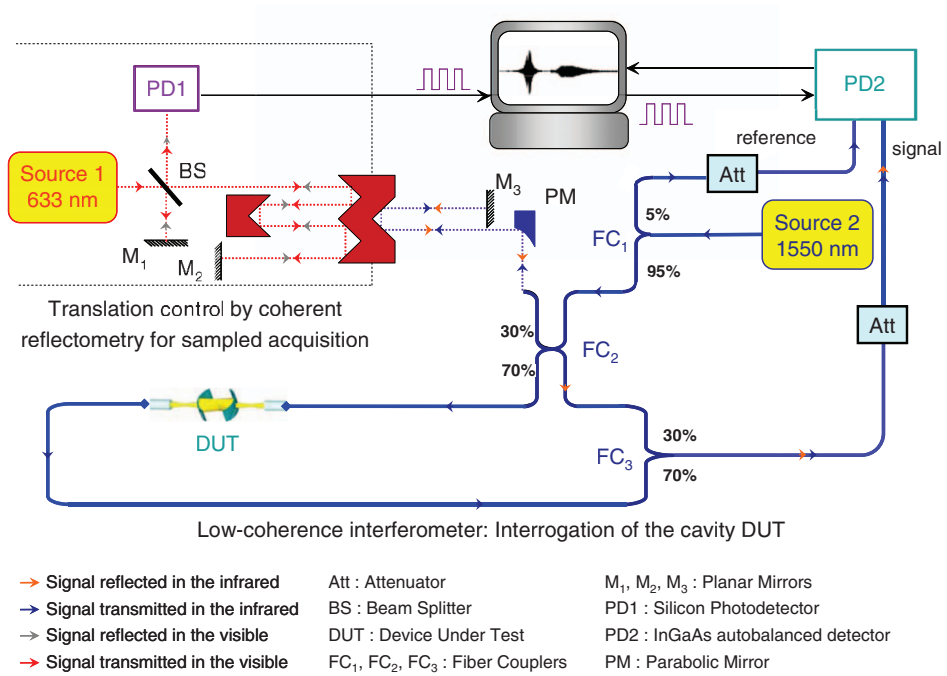

FIG. 3. Experimental setup illustrating the PS-OLCI measurement setup. The low coherence Michelson interferometer is associated with a broadband source and is used to test the Device Under Test (DUT). The upper coherent Michelson refeflectometer is coupled to the reference arm of the previous interferometer and helps acquiring the sampled synchronous acquisition of the measurement signal to obtain finally, both the amplitude and the phase response of the DUT.

TABLE I. Comparison between the physical lengths obtained using SEM and those obtained using the PS-OLCI. The measurements were carried-out on micromachined curved FP cavities based on two and three silicon layers per mirror.

		Cavity length L_{phys} (μm)	*Thickness of Silicon layer* t_{Si} (μm)	*Thickness of Air layer* t_{Air} (μm)	$2n_{Si}t_{Si} + 2t_{Air}$ (μm)	$4n_{Si}t_{Si} + 4t_{Air}$ (μm)
Device 1 based on	*SEM*	*210.0*	*3.61*	*3.55*	*32.2*	*64.4*
three layers per mirror	*PS-OLCI*	*210.0*	—	—	*30.4*	*65.6*
Device 2 based on	*SEM*	*210.0*	*3.61*	*3.55*	*32.2*	—
two layers per mirror	*PS-OLCI*	*209.8*	—	—	*31.0*	—

account the mean value of both physical and effective lengths ($<L_{phys}>$ and $<L_{eff}>$ respectively), as schematically depicted in Fig. 2. Therefore, it is indeed important to use lensed fibers and also to choose carefully their characteristics, including the spot size and hence, their Rayleigh range. The characterization procedure can be summarized as follows: once the alignment conditions have been optimized, the coherent interferometer is controlled remotely so that the reference mirror of the Michelson interferometer initiates its spatial scan while the power transmitted through the tested cavity is recorded simultaneously, giving the interferograms. When needed, Fourier Transform is applied to the data acquired in the spatial domain, to give the spectral response of the DUT.

Inspection of the spectral response of this first device reveals an experimental $FSR_{Exp}(\lambda)$ of 5.36 nm in the wavelength domain, which is different from the theoretically expected $FSR_{Theory}(\lambda)$ of 5.72 nm, calculated from the actual reference value of the cavity physical length $L_{phys} = 210\ \mu m$, obtained from SEM measurements.

Experimental results of the spatial interferogram recorded on Device 1 and the corresponding envelope are presented in Fig. 4. The interferogram envelope, shown in Fig. 5, was obtained on a second device based on two silicon Bragg layers per mirror (Device 2). The main interference peaks are relevant to the optical path difference δ inside the cavity, which relate to integer multiples of

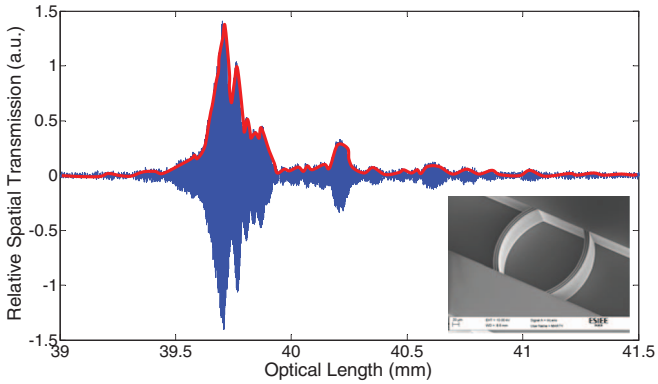

FIG. 4. Spatial interferogram of FP cavity based on three Bragg layers per mirror shown in the inset of the figure. The envelope of the spatial interferogram is highlighted.

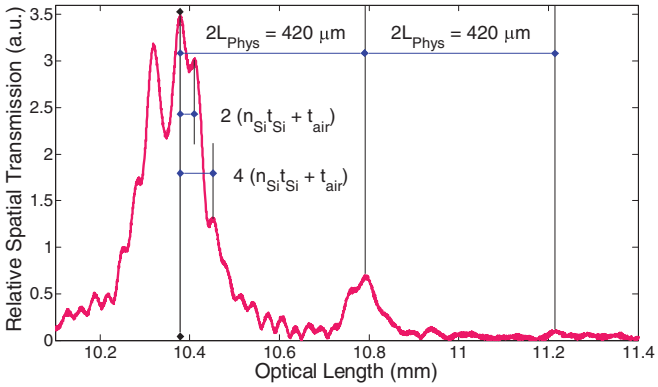

FIG. 5. Envelope of the spatial interferograms of FP cavity based on two Bragg layers per mirror (Device 2).

the physical length L_{phys} of the cavity. Moreover, there is a set of additional peaks, which relate to multiple reflections at the interfaces of the Bragg layers, as schematically depicted in Fig. 2(c). Hence, in addition to L_{phys}, more information can be extracted about the thicknesses and the number of the Bragg layers. The FP cavity dimensions extracted from Fig. 4. and Fig. 5. are summarized in table I. The thickness of silicon Bragg layers are obtained assuming a refractive index $n_{Si} = 3.478$ for single crystalline silicon at a wavelength of 1550 nm. While many other factors can affect the refractive index value such as the substrate doping type (n-type or p-type) and concentration levels as well as the environmental conditions (pressure and temperature), the combined effect of all these parameters has been evaluated and it was found to have a negligible impact ($\Delta n_{Si} \sim 0.001$ in the worst cases).

In PS-OLCI measurements, we concentrate on the difference between the peaks. Therefore, our concern is about relative positions to deduce the layer thickness or the cavity length, we do not consider however, absolute positions because we do not have a reference zero position. Inspection of the peaks in Fig. 4 and Fig. 5 reveals other secondary peaks located either on the right or on the left of the primary peak (which has the highest intensity). Actually, the secondary right peak observed in Fig. 4 pertains to a relative path difference of $4n_{Si}t_{Si} + 4t_{Air}$ ($\approx 60\ \mu$m) measured from the high peak amplitude and it is ascribed to double reflections between two silicon layers as illustrated in Fig. 2(c). A similar peak is observed in Fig. 5, with a path difference of 60 μm also pertaining to a path difference of $mL_{phys} + 4n_{Si}t_{Si} + 4t_{Air}$ but it is located here on the left side because the next higher peak might relate to a larger path difference of $mL_{phys} + 8n_{Si}t_{Si} + 8t_{Air}$ (m is an odd integer number that relates to transmission measurements). It is indeed only the difference between consecutive peaks that can give information about the physical length of the cavity or about the thicknesses of the layers.

Since the focus of this paper is about *the dimensional measurements,* we need to evaluate the accuracy of the method, in particular, for the thicknesses of the Bragg layers, which are the smallest dimensions in the FP cavities under consideration. For this purpose, we used a statistical approach in which we implemented four different experimental conditions, corresponding to different values of the optical power on the detector $P_{opt} = 50\ \mu$W, 100 μW, 200 μW and 368 μW. For each value of P_{opt}, the measurements have been repeated a minimum of 5 times and up to 10 times, leading to four data groups. For Device 2, we obtained a mean value of the optical thickness $<2n_{Si}t_{Si} + 2t_{Air} > = 31\ \mu$m with a reproducibility standard deviation of 0.67 μm, corresponding to a relative deviation of 2 %. These measurements also correspond to an error of 1.2 μm with respect to the reference value of 32.2 μm, that is a relative error of 3.7 %.

Secondly, planar FP cavities with longer optical path have been analyzed using the same setup. In these measurements, the first device is a two-side polished silicon substrate with sub-micron SiO_2 coating on both sides. The wafer thickness is known a priori to be 379 μm, corresponding to an optical path of 1318 μm. The cavity behaves as a low performance planar FP cavity based on thin film coating. Repetitive measurements using PS-OLCI leads to an optical path of 1342 μm, that is, a percentage error of 1.8 % with respect to the nominal value. PS-OLCI was also used to analyze a similar device, where the optical path is known a priori to be 1826 μm. The measured optical path using the PS-OLCI technique was found to be 1860 μm, that is with a percentage error of 1.9 %. The measurement error estimated on both devices is ascribed to the unavoidable angular misalignment of the DUT (along θ_x and θ_y) of about 7°, which leads to a slightly larger optical path than expected inside the cavity. It is worth to mention that the thicknesses of the thin film coating layers cannot be detected in this particular case because they fall below the detection limit of the implemented PS-OLCI technique, whose sensitivity is limited to optical paths slightly larger than few micrometers.

In conclusion, the PS-OLCI was successfully implemented for the dimensional characterization of micro-cavities having either curved or planar reflectors. The cavity physical length was retrieved, and this was the main motivation to conduct this research work. Hence, the discrimination from the effective cavity length, usually obtained from the spectral response through the *FSR*, can be done easily. In addition to the measurement of the cavity length, the use of PS-OLCI gave valuable information about the thickness and the number of layers of the cavity Bragg reflectors. The accuracy of the technique was also estimated in the order of 3.7 % and 1.9 %, for optical lengths of 30 μm and 1826 μm, respectively. The obtained results suggest that the proposed technique might be suitable to retrieve the dimensional characteristics of any device constructed from multiple dielectric layers. Then, the architecture of devices in closed packages can be determined with the help of reverse engineering based on the analysis of measurement data recorded using PS-OLCI, which allows, dimensional measurements of *a priori* unknown optical devices. However, it was shown that the applicable thickness range extends from 2 micrometers up to several hundreds of micrometers. To a certain extent, the proposed technique appears very complementary to ellipsometric measurements, when applicable.

[1] J. W. S. Rayleigh, Phil. Mag. **26**, 256 (1888).
[2] B. S. Kawasaki, K. O. Hill, D. C. Johnson, and Y. Fujii, Opt. Lett. **3**, 66 (1978).
[3] S. Wang, J. Appl. Phys. **44**, 767 (1973).
[4] H. Kogelnik and C. V. Shank, Appl. Phys. Letters **18**, 152 (1971).
[5] M. J. H. Marell, B. Smalbrugge, E. J. Geluk, P. J. van Veldhoven, B. Barcones, B. Koopmans, R. Nötzel, M. K. Smit, and M. T. Hill, Opt Express **19**, 15109 (2011).
[6] F. Koyama, S. Kinoshita, and K. Iga, Appl. Phys. Lett. **55**, 221 (1989).
[7] B. Weng, J. Ma, L. Wei, L. Li, J. Qiu, J. Xu, and Z. Shi, Appl. Phys. Lett. **99**, 221110 (2011).
[8] H. A. MacLeod, *Thin-Film Optical Filters* (Institute of Physics, Bristol, U.K., 2001).
[9] B. Saadany, M. Malak, M. Kubota, F. Marty, Y. Mita, D. Khalil, and T. Bourouina, IEEE J. Sel. Top. Quant. Electron. **12**, 1480 (2006).
[10] M. W. Pruessner, T. H. Stievater, and W. S. Rabinovich, Appl. Phys. Lett. **92**, 081101 (2008).
[11] A. Lipson and E. M. Yeatman, Opt. Lett. **31**, 395 (2006).
[12] M. Malak, N. Pavy, F. Marty, Y.-A. Peter, A. Q. Liu, and T. Bourouina, Appl. Phys. Lett. **98**, 211113 (2011).
[13] X. M. Zhang, H. Cai, C. Lu, C. K. Chen, and A. Q. Liu, in *Poceedings of the 19th IEEE International Conference on Micro Electro Mechanical Systems*, Istanbul, Turkey, 830, (2006).

[14] A. Q. Liu and X. M. Zhang, J. Micromech. Microeng. **17**, R1-R13 (2007).
[15] R. Gabet, P. Hamel, Y. Jaouën, A.-F. Obaton, V. Lanticq, and G. Debarge, J. Lightwave Technol **27**, 3021 (2009).
[16] A.-F Obaton, C. Palavicini, Y. Jaouën, E. Kerrinckx, Y. Quiquempois, and M. Lièvre, IEEE Trans. Instrum. Meas. **55**, 1696 (2006).
[17] C. Palavicini, Y. Jaouën, G. Debarge, E. Kerrinckx, Y. Quiquempois, M. Douay, C. Lepers, A.-F. Obaton, and G. Melin, Opt Lett. **30**, 361 (2005).